CompAct™ Arm: a Compliant Manipulator with Intrinsic Variable Physical Damping

Matteo Laffranchi, Nikos G. Tsagarakis and Darwin G. Caldwell

Fondazione Istituto Italiano di Tecnologia, Via Morego 30, 16163, Genova, Italy
{matteo.laffranchi; nikos.tsagarakis; darwin.caldwell}@iit.it

***Abstract*— Humans exploit compliance in their biomechanical muscle-tendon-bone actuation structure to enable robust and safe interaction with the environment and utilize the elastic energy stored into muscles and tendons to obtain large energy efficiency or high output mechanical power peaks at their limbs. From the robotic/mechatronic point of view it is clear that emulating such a property in robotic actuation systems enables the achievement of performance which is not possible with classical stiff designs. In contrast to this, transmission compliance introduces some disadvantages as e.g. typically underdamped modes which reduce the achievable control bandwidth, stability margin and accuracy of the controlled system. These limitations are solved in mammalians by means of physical damping which clarifies why these biological systems are able of performing fast and smooth yet accurate motions in their limbs. This motivates this work which consists in the analysis and development of the CompAct™ Arm, a novel compliant manipulator with intrinsic variable damping. This is probably the first robotic system to exhibit these diverse bio inspired characteristics. A motivation analysis is initially presented to show how the drawbacks introduced by compliance can be overcome by means of physical damping. The second part of the paper presents the mechatronic development of the robotic manipulator and preliminary experimental results.**

Keywords – Mechatronic Design, Compliant assembly, Bio-Inspired Design, Dynamics

I. INTRODUCTION

Improvements in production time and the quality of the products lie at the heart of modern manufacturing and the use of robots has formed an increasingly important aspect of the drive for efficiency. These robots are designed for precision, speed and repeatability and usually work in restricted areas to prevent any harmful interaction with humans. However, new opportunities are arising in houses and offices that mean that robots will not be confined to these relatively restricted factory environments and this sets new demands in terms of ability to interact with these less structured and more uncertain environments. It is evident that classical heavy and stiff manipulators with high control gains are not suitable to cooperate and work within these new operational areas. In fact, the typical design/control approaches mentioned previously make the resulting robots present serious interaction limitations and large output mechanical impedance which means that the robot and human safety are compromised when unexpected events occur. Yet, other aspects than safety can be jeopardized by this actuation approach as e.g. mechanical robustness and energy efficiency [1-3]. The reason for this is that rigid systems do not permit mechanical energy storage while compliant systems as e.g. humans' biological structures can exploit this property to improve the mentioned characteristics. These bio-inspired drives motivate scientists to attempt to replicate compliance within robots with a variety of solutions [1, 4-5].

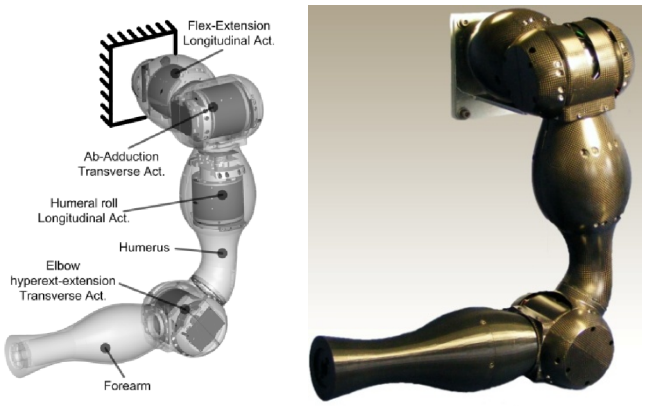

(a) (b)

Fig. 1 – The CompAct™ Arm: (a) external layout semi-transparent CAD view and (b) fully assembled prototype

Although compliance can effectively make the difference, from the engineering point of view it introduces also some side effects. It typically induces underdamped dynamics which deteriorate the stability margin and the accuracy of the robot (due to the induced oscillations) and limits the bandwidth which can be set in the controlled system [6-8]. These drawbacks are tackled in mammalians, which exhibit joint compliance, by the synergetic presence in their body of both compliance and physical damping. The properties of passive compliance and damping typical of biological joints explain why e.g. humans are able to safely interact and be robust during collision due to compliance while at the same time having the potential of achieving fast, smooth yet accurate motion thanks to physical damping, [9-11].

From the design perspective, it can be concluded that the introduction of damping in the mechatronics of the compliant robot joints (possibly with the ability of varying its level) can be a solution to overcome the drawbacks

This work is supported by the European Commission project SAPHARI FP7-ICT-287513.

introduced by compliance. Apart from this, previous work demonstrated that physical damping can enhance the dynamic performance and accuracy of force-torque controlled systems [12]. Although some of the mentioned advantages are obvious, a rigorous analysis is necessary to clarify in depth the role of physical damping in compliant robotic joints.

This paper proposes in its first part an analysis on the effects of physical damping in compliant robotic joints assessing how this parameter affects the dynamic performance, energy efficiency and safety of compliant actuators. The positive outcome of this study motivated the design and development of the CompAct™ Arm, i.e. a manipulator powered by actuators with intrinsic rich skills related to the synergetic combination of passive compliance and variable physical damping. To the authors knowledge this is the first robotic systems to exhibit these combined properties. We believe that such a system is step towards the achievement of functional performance of natural systems and particularly the human in terms of motion agility, safety, energy efficiency and power. The mechatronic details of this highly integrated system are presented in the second part of this paper.

The paper is structured as follows: Section II presents an analysis to evaluate and quantify how physical damping affects the characteristics of a generic compliant actuator while Section III introduces the mechatronic details of the actuation units employed for the development of the manipulator. Section IV defines the kinematic layout of the robot and analyses a dynamic simulation involving an interactive task for determining the preliminary specifications of the manipulator and related actuation systems. The robot assembly and design is analysed in Section V, with Section VI presenting preliminary results obtained with the prototype. Finally, Section VII addresses the conclusions and future work.

II. Dynamics of Compliant Actuation Systems with Intrinsic Variable Damping

A. Mechanical model

Considering the basic equivalent linear model of a compliant actuator, Fig. 2a, the system dynamics can be expressed by the following set of equations:

$$\begin{aligned} M_R\ddot{x_\theta} + D\left(\dot{x_\theta} - \dot{x_q}\right) + K\left(x_\theta - x_q\right) &= F_{in} \\ M_L\ddot{x_q} - D\left(\dot{x_\theta} - \dot{x_q}\right) - K\left(x_\theta - x_q\right) &= F_{out} \end{aligned} \quad (1)$$

where M_R = 0.5 kg and M_L = 1 kg are the reflected rotor and equivalent link inertias, D and K = 100 N/m are the joint viscous damping and stiffness, x_θ and x_q are the rotor and link equivalent linear displacement, F_{in} and F_{out} are the effort provided by the actuation system and the force applied to the outer link, respectively. The basic model presented in Fig. 2a makes some assumptions, i.e. it does not consider any dissipative effect (such as e.g. friction/damping due to the gearbox, bearings, etc. or due to joule losses in the resistance of the drivers/windings) apart from that of the transmission damper D and neglects the electrical (or hydraulic) dynamics of the driving system. In fact, these hypotheses are made on purpose to make the analyses independent of the specific nature of the actuator and make the analysis and results more generalised.

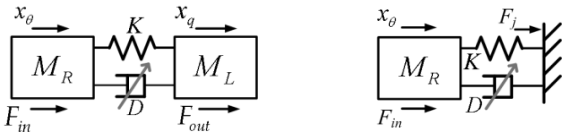

(a) (b)

Fig. 2 – (a) Equivalent model of a SEA with variable physical damping and (b) model of the constrained collision scenario

B. Dynamic performance

Assuming no interaction is involved (F_{out} = 0N), the following transfer function between rotor and link velocity (V_θ and V_q) can be obtained from (1):

$$P(s) = \frac{V_q}{V_\theta} = \frac{Ds + K}{M_L s^2 + Ds + K} \quad (2)$$

In fact, an increase of the variable joint viscous damping D of the system in Fig. 2a, can be increased to shift the zero of (2) to lower frequencies to introduce a phase lead action (typically from resonance to approximately 2 decades after) avoiding the sharp and significant phase lag introduced by the complex conjugate poles caused by compliance[1]. This improves the stability of the system hence facilitating the link position/velocity control. At the same time, the damping D can be set sufficiently large so as to reduce the amplitude of the oscillations of the vibration modes and facilitate accurate position tracking when needed. In addition to this, the magnitude of (2) increases with joint damping in the high frequency domain above resonance. From the performance perspective this is a further attractive feature since this means that for a given actuation system the maximum output speed limit increases at certain operating frequency (above resonance).

The high frequency performance improvement gained by a joint damping increase can be quantified by the following coefficient:

$$G_D = \lim_{\omega\to\infty} \frac{\|P^+(s=j\omega)\|}{\|P^-(s=j\omega)\|} = \frac{D^+}{D^-} \quad (3)$$

where P^+ and P^- are plants having the form of (2) and featuring two different levels of joint damping D^+ and D^- such that $D^+ > D^-$. Equation (3) shows that G_D increases proportionally with joint damping meaning that dynamic performance can be augmented by means of damping.

C. Energy efficiency

Considering the system in Fig. 2a, the rotor velocity v_θ required to produce certain link motion can be computed using (2), while the required actuator force F_{in} is obtained using (1). The corresponding mechanical power input P_{in}

[1] In fact, compliance acts as a limiting factor to the dynamic performance which can be achieved in the controlled system. As a rule of a thumb, the bandwidth of closed loop (lightly damped) systems should be placed below 1/3 of the mechanical poles introduced by compliance, [6].

required to provide a desired link velocity can therefore be computed in the frequency domain as:

$$P_{in}(s) = F_{in}(s) * V_{\theta}(s) \quad (4)$$

Considering a required velocity output of amplitude 0.1 rad/s, the required RMS power input as a function of the frequency is shown in Fig. 3 for different physical viscous damping levels. It can be observed that the effect of damping on the power consumption varies in function of the operating frequency, that is, in the low frequency domain (approximately in the range of [0, 1]Hz for this specific system) there is no substantial change varying damping; whereas systems with small damping are much more energy efficient in proximity of resonance.

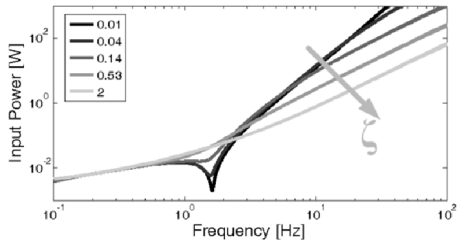

Fig. 3 – Input mechanical power consumption required to provide an output velocity of amplitude 0.1 rad/s for different damping ratio values as a function of the operating frequency.

This last effect is quite obvious since the system is exploiting its natural dynamics to perform the motion. In contrast to this, it is quite surprising that systems with high joint physical damping feature much higher energy efficiency than compliant actuators with low joint viscous friction in the high frequency domain. This is due to the fact that motor and link in compliant actuators are highly decoupled in the high frequency domain and therefore in this region much more effort is required on the motor side to compensate for this decoupling effect when damping is low [13]. In other words, compliance can be beneficial from the efficiency perspective when the system operating frequency matches the natural dynamics (as in e.g. [1]), however when the task requires higher frequency motions the system has to work against the physics of the system hence compromising energy efficiency[2]. This in turns means that physical damping can be attractive especially in fixed stiffness designs (as e.g. SEAs) where dynamics cannot be tuned: a tunable damper placed in parallel to the transmission compliance can be an effective mean for the development of performing and efficient (at high frequency spectrum) compliant actuators.

D. Safety

The higher dynamic performance and energy efficiency achieved in plants with larger physical viscous damping level demonstrated previously is due to the increased coupling between rotor and link. This is on one hand an attractive property of physical viscous damping, however on the other hand this quantity introduces the side effect of a decreased safety level due to the generation of higher forces at impact. To evaluate this effect, we consider here the risky case of a constrained collision of the system in Fig. 2b, [14]. This scenario is modelled as in Fig. 2b with the purpose of characterizing the joint force generated at collision.

A transfer function which can be used for the evaluation of the safety is the force transmissibility between the input and joint force[3]. For the system in Fig. 2b, this function is:

$$T(s) = \frac{F_j}{F_{in}} = \frac{Ds + K}{M_R s^2 + Ds + K} \quad (5)$$

This transfer function has the same form of (2), apart from the fact that the reflected mass appearing at denominator is that of the rotor instead of that of the link. This means that (3) is valid also for (5), that is, the same amount of improvement gained in performance is lost in safety. In fact, this does not represent a problem because if the actuator has the possibility of varying the joint physical damping level as in the systems of Fig. 2, this parameter can be adjusted to an optimal value as a function of the system states and of the required safety level (as in e.g. the fast and soft paradigm, [5]) to obtain the best safety-performance tradeoff.

III. MECHATRONICS OF THE ACTUATION SYSTEMS

A. Damping systems

Dampers can be categorized in three main classes: passive, active [15] and semi-active [7, 12] basing on the amount of external power required for the damping control system to perform its functionality. Purely passive dampers are not able to adapt the damping value in function of the system configuration/state, while active dampers can be employed to suppress oscillations however they do not offer the benefits analysed in the previous section. On the other hand, semi-active solutions offer the reliability of passive devices while at the same time maintain the versatility and the adaptability of active systems without requiring large amount of energy [7]. In addition, differently from active implementations, they cannot inject mechanical power into the system and therefore they do not have the potential of destabilizing the controlled actuator. When appropriately controlled semi-active systems perform significantly better than passive devices and have the potential of achieving the majority of the performance of the fully active configuration (e.g. ability of regulation of the damping level over wide ranges) [7]. Furthermore, a semi-active damping system can be completely disconnected in particularly critical conditions to maximize the decoupling effect of compliance, such as e.g. when the robot is working in close proximity of the human/environment. This suggests that the use of an actuation system which can provide passive compliance and variable physical damping (using e.g. a semi active damper) can effectively be employed to develop human-friendly and

[2] It is worth mentioning that this effect can be observed also in the time domain for tracking profiles whose dominant spectral components are well below the system natural frequency [13].

[3] In this work we do not consider the contribution to the impact force of the reflected link mass since this variable is independent from the transmission viscous damping and stiffness.

still well performing robots and is therefore employed in the actuation modules used for the development of the manipulator presented in this work.

B. The modular design concept

Looking at the kinematics of existing serial robots e.g. the Comau Smart NM, [16], Barrett WAM, [17], but also humanoid robots as the Honda ASIMO, [18], Figs. 4a, b, it can be observed that their kinematic structure is mainly composed of revolute joints placed in two different configurations.

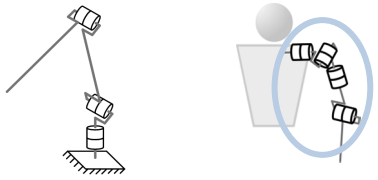

(a) (b)

Fig. 4 –Conceptual schemes showing the kinematics of (a), Comau Smart NM, (b) Honda ASIMO and Barrett WAM manipulators.

The first actuator kinematic configuration counts the joint axis aligned with the robot structure (this configuration is defined as "longitudinal joint" in this work), whereas the second arrangement is represented by the joint axis placed perpendicularly to the robot structure, which is instead defined as "transverse joint" configuration. For instance, the Comau robot shown in Fig. 4a is made of a longitudinal-transverse-transverse configuration while the ASIMO robot arm, Fig. 4b, presents a kinematic chain made of a longitudinal-transverse-longitudinal-transverse arrangement.

From the analysed examples of Fig. 4, it can be concluded that from the kinematic perspective a serial robot uses mostly revolute joints placed in two basic configurations: the longitudinal and the transverse joints. A serial robot design can therefore be developed by means of an appropriate serial combination of these two joint configurations. The employed actuation system is a series elastic actuator which presents the ability of regulating the physical damping in parallel to the joint compliance and is therefore suited for the development of this manipulator [8]. The adjustment of the damping is realized by a semi-active friction damper actuated by light and compact piezoelectric stack actuators[4], Fig. 5b. Based on the modular design concept the actuation units were formatted following the Longitudinal and Transverse kinematic schemes for developing the full arm. To satisfy the lightweight property of the overall arm a carbon fibre frame was used in this design. The mentioned structure is used not only as frame but also as a cover preventing the human/environment to enter in contact with the mechatronics of the manipulator therefore improving its robustness and safe properties. A further attractive aspect of the use of composite material is that in contrast to traditional manufacturing processes as milling or sheet metal forming it facilitates the development of parts without sharp edges which may result unsafe during interaction. The highly integrated modules embed all the mechatronics of the system including motor-gearbox group, series compliant joint, semi-active damping system, control and conditioning electronics.

1) Longitudinal actuation module

The design of this module is shown in Fig. 5. The actuation system is fixed to the carbon fibre frames in two points, i.e. at the base and front support flanges of the actuator, Fig. 5a. This is to avoid the application of thrust moments to the actuator which may result in malfunction due to the misalignment between the frictional surfaces of the damping system, Fig. 5b. The input interface is an aluminium disk which is directly connected to the frame by means of structural adhesive while the output interface is an aluminium component machined with a geometry which is the negative of that of the input disk. The thickness of the carbon fibre frame has been dimensioned to 1.5mm which guarantees sufficient strength of the structure when the nominal load is applied to the fully extended arm and has been validated by means of finite elements analysis (FEM). The achievable range of motion for this joint is $[0, 2\pi]$ rad, although its motion can be constrained on demand to shorter ranges by means of mechanical locks. The total weight of the unit is m_S = 2.2 kg. The fully assembled module is shown in Fig. 7a.

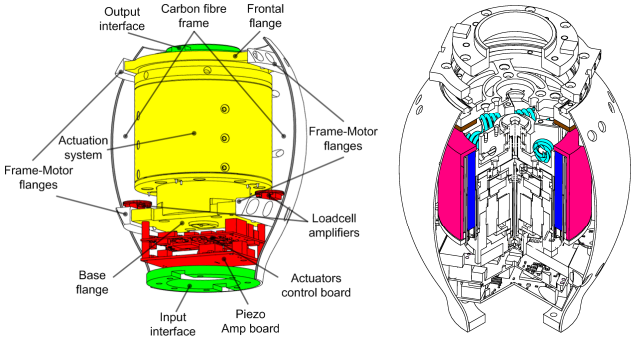

(a) (b)

Fig. 5 – (a) Open view (yellow: actuation system, red: electronics, green: input-output interfaces) and (b) semi-exploded cross section view of the longitudinal actuation module (dark blue: piezoelectric stacks of the VPDA, light blue: springs of the compliant module, pink and brown: frictional surfaces of the VPDA). For more details on this design, please refer to [8].

2) "Transverse" actuation module

In the transverse configuration the frame has been designed in order to allow the replication of the kinematic configuration mentioned previously. Similarly as in the longitudinal module, the actuator is supported on both sides by means of the base and front flanges for the same reasons previously explained, Fig. 6. The input and output mechanical interfaces present the same geometry as that of the longitudinal module in order to fulfil the modular property and permit arbitrary interconnections between the

[4] The use of semi-active damping systems placed between the actuator and the load is not a new concept in robotics, see e.g. [12, 19]; however these works do not make use of mechanical compliance. In fact dampers in these works are employed as transmission systems (similarly as clutches) and they are hence used to deliver the actuator effort to the load. This means that these systems typically suffer of low energy efficiency when compared to SEAs/VSAs or hybrid solutions as that presented in this work, [12].

modules. In this case the thickness of the carbon fibre structure is 1.5mm as well as in the previous case whereas the maximum achievable range of motion for this joint is $[-\pi/2, \pi/2]$ rad and its total weight is $m_T = 2.4$ kg. The fully assembled prototype is shown in Fig. 7a whereas its specifications are reported in Tab I together with those of the longitudinal module.

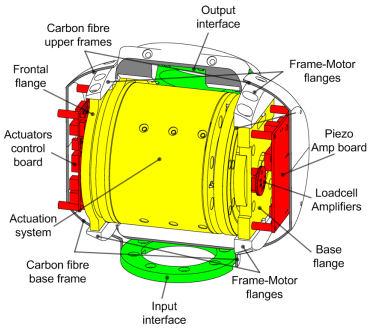

Fig. 6 – Open view of the transverse actuation module (yellow: actuation system, red: electronics, green: input-output interfaces). For the mechanical design of the actuation system refer to Fig 5b and to [8].

TABLE I
SPECIFICATIONS OF THE LONGITUDINAL AND TRANSVERSE ACTUATION MODULES

Parameter	Value
Gear ratio – N	100
Power	190 W
Maximum output continuous torque	40 Nm
Maximum joint velocity	10.7 rad/s (≈ 610 °/s)
Maximum rotary passive deflection	±0.18 rad
Maximum damping torque	9 Nm
Joint stiffness	188 Nm/rad
Joint Damping Range	[0, 9] Nms/rad
Inherent joint viscous damping	0.25 Nms/rad
Total mass of the longitudinal actuator - m_S	2.2 kg
Total mass of the transverse actuator - m_T	2.4 kg

(a) (b) (c)

Fig. 7 – (a) Longitudinal (left) and transverse (right) actuation modules, (b) Actuators control board and (b) Piezo amplifier board

C. Sensing and electronics

Regarding the available sensors, both modules are equipped with an incremental 12-bit position encoder placed on the motor shaft and two magnetic 12-bit absolute encoders to monitor the compliant module deflection angle and the mechanical angle of the motor after the reduction drive. A strain gauge – based custom made force sensor is machined on the actuator structure to permit the measurement of the force applied by the piezo actuators, whereas a custom made torque sensor which exploits the same sensing principle is assembled at the output of the harmonic drive gear to measure the joint torque. Each module is provided with a motor control board, Fig. 7b, used for the sensor data acquisition, control of the whole unit and generation of the command voltages for the brushless DC motor and the piezoelectric driver amplifier board, Fig. 7c. This latter board is used for amplifying the control signals for the piezo stack actuators of the employed friction damper in the nominal voltage range of [0, 150]V as required by the piezos. The communication with the controller is performed through a 100Mbit Ethernet interface utilizing both TCP and UDP protocols.

IV. MANIPULATOR SPECIFICATIONS

Among the most important issues to be addressed when considering anthropomorphic/humanoid design is the definition of the basic layout of the robot. This phase includes the definition of the kinematics and dimensions of the arm which guarantee an appropriate nominal payload at the same time permitting an overall natural and proportioned design. The size of the manipulator is approximately that of an adult human arm. Regarding the kinematics, three degrees of freedom are located at the shoulder complex and complemented by an additional degree of freedom for the implementation of the elbow flexion-extension DOF. The first three DOFs will reproduce, in sequence, the arm extension-flexion, adduction-abduction and humeral roll degrees of freedom accordingly with the ball-socket kinematic shoulder model, [20]. The elbow pronation-supination degree of freedom is not implemented in this first manipulator version since this degree of freedom plays a less important role in the physical human robot interaction and therefore the inclusion of compliance (and related variable physical damping) is likely not strictly necessary for this specific degree of freedom. The average ranges of motions of the adult human arm are used as a starting point for the selection of the moveable ranges of each joint of the manipulator. These are reported in Tab. II, [20][5].

A. Static analysis

Although an arm with dimensions exactly equal to those of a 50th percentile male can be designed by means of the modules presented in Section III, these dimensions have equally been increased with the purpose of making the manipulator layout proportioned at the same time guaranteeing that the actuators are capable of delivering the required torque. Statically, the configurations with fully extended arm on the transverse plane are the worst case layouts since the arm centre of mass is distal hence

[5] Note that the ranges of motion reported in Tab. II have been slightly extended with respect to those of the human arm

maximizing the lever arm of the moment produced by gravity. The worst case load scenarios of the manipulator are shown in Fig 8. The two cases of Fig. 8 are equivalent due to the properties of the roll-pitch-roll joint employed for the development of the shoulder and this allows finding a unique solution to the dimensioning problem.

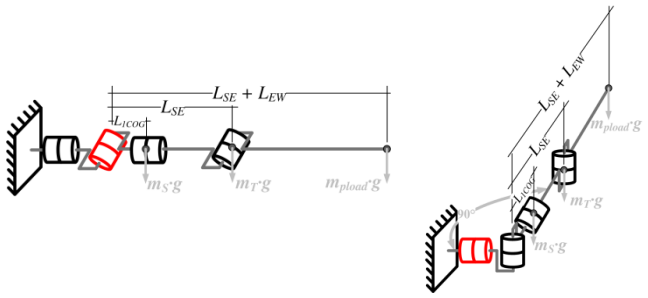

(a) (b)

Fig. 8 – Worst case load configurations of the arm. In the configuration of (a) the shoulder adduction-abduction actuator receives the maximum load, while for (b) the most stressed actuator is that of the flexion-extension DOF

The equilibrium equation of the static torque due to gravitational forces at the critical actuators (shown in red in Fig. 8) is:

$$T = L_{1COG} \cdot m_S \cdot g + L_{SE} \cdot m_T \cdot g + L_{SE} \cdot P \cdot m_{pload} \cdot g \qquad (6)$$

where T is the torque applied to the critically loaded actuators, L_{1COG} is the distance between the point of intersection of the axes of the DOFs of the shoulder (defined as p_{SH}) and the centre of gravity of the humeral roll actuator and is given by the dimensions of the mechanical assembly of the longitudinal and transverse actuation modules. L_{SE} represents the distance between p_{SH} and the centre of gravity of the elbow flexion-extension DOF whereas g is the acceleration of gravity and $P = 1.8$ is the ratio between the total arm and the humerus lengths ($P = [L_{SE}+L_{EW}]/L_{SE}$ using the notation of Fig. 8) of a 50th percentile adult male, [21].

TABLE II
SPECIFICATIONS AND RANGES OF MOTIONS (ROM) OF THE MANIPULATOR

Parameter	Value
Arm base – shoulder axes intersection distance (L_{BS})	$193 \cdot 10^{-3}$ m
Shoulder axes intersection – elbow axis distance (L_{SE})	$393 \cdot 10^{-3}$ m
Elbow axis – wrist axes intersection distance (L_{EW})	$360 \cdot 10^{-3}$ m
Total weight (m_{arm})	9.9 kg
Nominal static load at the EE @ extended arm (m_{pload})	4 kg
Arm extension-flexion ROM	[-45, 180]°
Arm adduction-abduction ROM	[0, 170]°
Humeral roll internal-external rotation ROM	[-90, 90]°
Elbow flexion-extension ROM	[0, 145]°

Setting the payload to m_{pload} = 4kg and considering that the critical actuators are loaded at their maximum torque value (Tab I) and solving (6) with respect to L_{SE} it is possible to obtain the value of this parameter while the total arm length can be set by means of the scaling factor P

$$L_{SE} + L_{EW} = P \cdot L_{SE} \qquad (7)$$

where L_{EW} is the distance between the elbow and the wrist axes. Considering the specified payload the layout of the arm is proportionally scaled with a factor of approximately 40% with respect to the dimensions of a 50th percentile human arm, [21]. At the same time, such a nominal payload will permit the assembly of a hand/gripper at the robot end effector still leaving some load margin. The overall dimensions, mass and nominal payload of the manipulator are reported in Tab. II.

B. Dynamic and interaction analysis

Using the determined kinematic layout and the physical properties (e.g. mass, stiffness) reported in Tab. I and II as a baseline, dynamic simulations have been carried out to give an indication of the typical torque/velocity profiles required by the employed actuation system when the arm is performing a task which requires physical interaction. A further mass of weight 2 kg has been applied to the end effector to simulate a load and/or the mass of a robotic hand/gripper. As an example case, we analyse here the previously studied task of a manipulator writing on a blackboard, [22], Fig. 9.

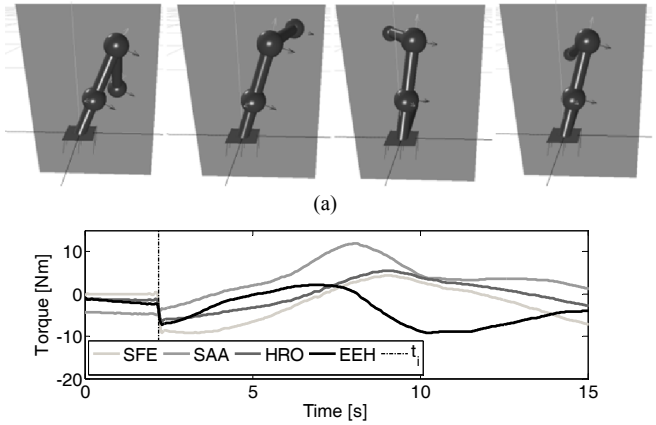

(a)

(b)

Fig. 9 – (a) Snapshot sequence of the simulation animation (manipulator 3D model in black and blackboard in grey) and (b) torques required for the execution of the task. The acronyms SFE, SAA, HRO, EFE represent the Shoulder Flexion-Extension, Shoulder Abduction-Adduction, Humeral Roll and Elbow Flexion Extension DOFs while t_i is the instant when interaction begins.

The joint trajectory data obtained from the experiments in [22][6] were imposed to the motor positions of the manipulator model to obtain the required joint torques (which result from gravity, dynamics and interaction). A virtual rigid wall simulating the blackboard was implemented in the simulator to generate normal reaction forces on the manipulator end effector when interaction was verified. The joints torques required for the execution of this task are shown in Fig. 9b. Figure 9b shows that before interaction (this occurs at t_i = 2.2s), the required torques reach relatively small magnitude levels, i.e. a maximum amplitude of approximately 5 Nm in the shoulder abduction-

[6] We use this example case as the Barrett WAM arm employed for the experiments in [22] presents a kinematic layout which is very much similar to that of the arm presented in this paper.

adduction joint. This occurs because in this phase the actuators compensate for the gravity and the inertial torques only. However, after this instant the torques increase in magnitude due to the increased effort required by the interaction. It is important to notice that the torques of Fig. 9b correspond to the effort required to perfectly track the desired motor positions and therefore can represent a scenario where high gain motor position controllers are implemented. This hence constitutes a worst case situation since robots designed for interaction should employ safety-oriented controllers which can adapt the robot configuration to limit the interaction force/torque.

The maximum output velocity required by the actuators in the execution of this task is 0.42 rad/s and is reached by the elbow joint. The obtained maximum velocities and torques are much lower than the nominal values which can be generated by the actuators, Tab. I, demonstrating that such an interaction task can be executed by the presented system with large torque and velocity safety margins.

V. Manipulator Assembly and Kinematics

A roll-pitch-roll "spherical" joint made of the series longitudinal-transverse-longitudinal forms the shoulder of the manipulator. Assembled to this, a hollow carbon fibre part defined as "Humerus" is used to connect the shoulder to the elbow. The Humerus output interface has been inclined of 50 degrees with respect to its input flange to respect the set range of motion specifications, Tab. II. The output flange of the Humerus is connected with the input interface of another transverse actuator which implements the elbow flexion-extension degree of freedom. Finally, a hollow part implements the manipulator forearm hence completing the design of the arm.

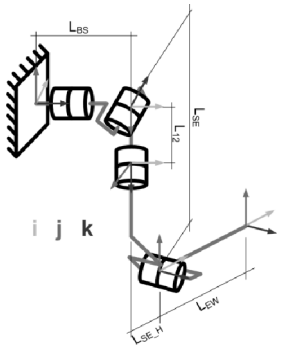

Fig. 10 – (a) Kinematics of the manipulator and reference frames according to the Denavit-Hartenberg convention. The frame shown at the manipulator base is used as "home" configuration for the DH parameters.

TABLE III
D-H PARAMETERS OF THE MANIPULATOR

Link ID	D	θ	a	A
1	L_{BS}	$(3/2)\,\pi + q_1$	0	$(3/2)\,\pi$
2	L_{12}	$(3/2)\,\pi - q_2$	0	$(3/2)\,\pi$
3	L_{SE}	$(3/2)\,\pi + q_3$	L_{SE_H}	$(3/2)\,\pi$
4	0	q_4	L_{EW}	0

This latter part is designed so as to permit the future integration of a robotic hand. The full arm design is shown in Fig. 1. A schematic summarizing the kinematics of the manipulator is shown in Fig. 10 whereas their Denavit-Hartenberg parameters are reported in Table III.

The ranges of motion reported in Tab. II are implemented by means of a mechanical pin-based locking mechanism which is employed in each joint of the arm.

VI. Experimental Results

Preliminary results are presented in this section as proof of concept of the employed actuation system applied to the presented design. A weight of mass 3kg was assembled at the link extremity of an experimental prototype version of the actuation modules shown in Fig. 7 in order to replicate a moment of inertia of J_L = 0.13 kg·m^2 which simulates the load of a possible robot configuration (it is about one third of the highest moment of inertia which can be reached by the manipulator, i.e. that seen by the proximal actuator for the fully extended arm, J_{arm} = 0.42 kg·m^2 ≈ 3J_L). A step position reference of amplitude 0.15 rad (8.6°) was sent to the position-controlled motor in order to induce oscillations to be damped by the semiactive damper while the link position was recorded, Fig. 11. It is important to remark that no controllers to shape the dynamics (as e.g. impedance/admittance control) were implemented on the motor which was controlled using pure position control in order to show the action of the full module with the variable physical damper which is regulated using the viscous damping control scheme proposed in [8]. At the same time, two levels of desired joint physical damping (corresponding to damping ratios of ζ_1 = 0.3, ζ_2 = 1[7]) were sent to the damping system in order to show the ability of the damping module in the dynamic replication of the desired joint physical damping, Fig. 11. The experimental data obtained in Fig. 11a has been compared with simulation results to validate the effectiveness of the system mechatronics.

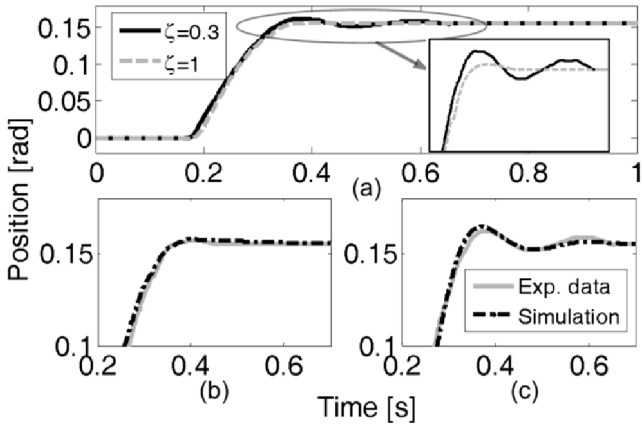

Fig. 11 – (a) Recorded link position step responses of the actuation system for different levels of joint physical damping and overplots of the experimental results shown in (a) with the simulation results of the (b) high and (c) low damping cases.

[7] Note that this quantity is intended in this paper as the equivalent damping ratio of the mass spring damper system formed by the damped compliant joint and the link inertia (locked system).

The simulated link position data was obtained by using the recorded motor trajectory in the experiments shown in Fig. 11a as a source of flow for an equivalent mass-spring-variable damper system which simulates the joint-link assembly. These have been plotted together with the experimental link position data either for a low (D_1 = 1.48 Nms/rad, ζ_1 = 0.3) and high (D_2 = 9.89 Nms/rad, ζ_1 = 1) joint viscous damping levels, Figs. 12b and 12c, respectively. The resemblance between simulated and experimental data is clear, however nonlinearities such as e.g. dry friction due to the bearings and assembly have not been considered into the model used for the simulation and this creates slight estimation errors.

VII. Conclusions and Future Work

This paper presented the analysis and development of the CompAct™ Arm, i.e. a highly integrated compliant manipulator with intrinsic variable physical damping. The positive results obtained in the first part of the paper demonstrated that joint physical damping has a significant positive effect in the dynamic performance, accuracy and efficiency (in the high frequency domain) of compliant robots. This motivated the employment of a piezoelectrically actuated semi-active friction damper in parallel to the transmission compliance of the actuation system. The resultant manipulator is probably the first robotic system to exhibit these rich bio-inspired physical properties making a step towards the development of robots with enhanced capabilities and performance approaching those of biological systems and in particular of the human.

In addition, this anthropomorphic manipulator presents low weight (thanks to the compact design and carbon fibre frame) and joint compliance at all DOFs with the objective of realising high interaction-related performances, enhance robustness and safety. It is developed following a modular design concept, i.e. the use of highly integrated actuation modules which embed the whole actuator mechatronics. The obvious advantage of such a design approach is its versatility, which facilitate the development of further robots (e.g. full humanoids) by employing the two presented modules. The intrinsic characteristics of the presented system (lightweight, joint compliance and variable physical damping) will make this robot able to interact with the environment presenting at the same time robustness, good accuracy and dynamic performance.

Further experiments will be carried out on the full manipulator to show the benefits of the introduced damping as demonstrated in the first part of the paper and to fully characterise the effects of damping on safety. Future developments will also include the design of novel control strategies intended to fully exploit the functionalities and advantages of the incorporated semiactive damping system.

VIII. References

[1] A. Jafari, N. G. Tsagarakis and D. G. Caldwell, "Exploiting Natural Dynamics for Energy Minimization using an Actuator with Adjustable Stiffness (AwAS)," in *International Conference on Robotics and Automation*, Shanghai, China, 2011.

[2] A. M. Dollar and R. D. Howe, "A robust compliant grasper via shape deposition manufacturing" *Mechatronics, IEEE/ASME Transactions on,* vol. 11, no. 2, pp. 154-161, 2006

[3] M. Laffranchi, N. G. Tsagarakis, F. Cannella and D. G. Caldwell, "Antagonistic and series elastic actuators: a comparative analysis on the energy consumption," in *Intelligent Robots and Systems (IROS). IEEE/RSJ International Conference on*, St. Louis, USA, 2009, pp. 5678-5684.

[4] M. G. Catalano, G. Grioli, M. Garabini, F. Bonomo, M. Mancini, N. G. Tsagarakis and A. Bicchi, "VSA - CubeBot. A modular variable stiffness platform for multi degrees of freedom systems," in *International Conference on Robotics and Automation*, Shanghai, China, 2011, pp.

[5] A. Bicchi and G. Tonietti, "Fast and soft arm tactics." *Ieee Robotics & Automation Magazine,* vol. 11, no. 3, 2004

[6] A. De Luca and W. Book, "Robots with Flexible Elements" *Handbook of Robotics*, S. K. Editors, ed.: Springer, 2008.

[7] M. Laffranchi, N. G. Tsagarakis and D. G. Caldwell, "A variable physical damping actuator (VPDA) for compliant robotic joints," in *Robotics and Automation (ICRA), IEEE International Conference on*, Anchorage, USA, 2010, pp. 1668-1674.

[8] M. Laffranchi, N. G. Tsagarakis and D. G. Caldwell, "A Compact Compliant Actuator (CompAct™) with Variable Physical Damping," in *International Conference on Robotics and Automation (ICRA)*, Shanghai, China, 2011, pp. 4644-4650.

[9] T. E. Milner and C. Cloutier, "Damping of the wrist joint during voluntary movement" *Experimental Brain Research,* vol. 122, no. 3, pp. 309-317, 1998

[10] H. Gomi and R. Osu, "Task-Dependent Viscoelasticity of Human Multijoint Arm and its Spatial Characteristics for Interaction with Environmentsq" *J. Neuroscience,* vol. 18, no. 21, pp. 8965-8978, 1998

[11] T. Tsuji, Y. Takeda and Y. Tanaka, "Analysis of mechanical impedance in human arm movements using a virtual tennis system" *Biological Cybernetics,* vol. 91, no. 5, pp. 295-305, 2004,10.1007/s00422-004-0515-1.

[12] C. Chee-Meng, H. Geok-Soon and Z. Wei, "Series damper actuator: a novel force/torque control actuator," in *Humanoid Robots, 2004 4th IEEE/RAS International Conference on*, 2004, pp. 533-546 Vol. 2.

[13] M. Laffranchi, N. G. Tsagarakis and D. G. Caldwell, "Analysis and Development of a Semiactive Damper for Compliant Actuation Systems" *IEEE/ASME Transactions on Mechatronics*, 2012, 2012,10.1109/TMECH.2012.2184293.

[14] M. Laffranchi, N. G. Tsagarakis and D. G. Caldwell, "Safe human robot interaction via energy regulation control," in *Intelligent Robots and Systems (IROS). IEEE/RSJ International Conference on*, St. Louis, USA, 2009, pp. 35-41.

[15] J. Y. Lew and S. M. Moon, "A simple active damping control for compliant base manipulators" *Mechatronics, IEEE/ASME Transactions on,* vol. 6, no. 3, pp. 305-310, 2001

[16] http://www.comau.it/,

[17] http://www.barrett.com/robot/index,

[18] M. Hirose and K. Ogawa, "Honda humanoid robots development" *Philosophical Transactions of the Royal Society A: Mathematical, Physical and Engineering Sciences,* vol. 365, no. 1850, pp. 11-19, January 15, 2007, 2007,10.1098/rsta.2006.1917.

[19] A. S. Shafer and M. R. Kermani, "Design and Validation of a Magneto-Rheological Clutch for Practical Control Applications in Human-Friendly Manipulation," in *Robotics and Automation, International Conference on*, Shanghai, China, 2011, pp. 4266-4271.

[20] V. M. Zatsiorsky, *Kinematics of Human Motion*, Leeds, UK Human Kinetics Pub., 1998.

[21] A. R. Tilley and H. D. Associates, *The Measure of Man and Woman: Human Factors in Design*, Whitney Library of Design, 1993.

[22] A. Pistillo, S. Calinon and D. G. Caldwell, "Bilateral Physical Interaction with a Robot Manipulator through a weighted Combination of Flow Fields," in *International Conference on Intelligent Robots and Systems*, San Francisco, CA, USA, 2011.